We are IntechOpen, the world's leading publisher of Open Access books
Built by scientists, for scientists

6,000
Open access books available

148,000
International authors and editors

185M
Downloads

Our authors are among the

154
Countries delivered to

TOP 1%
most cited scientists

12.2%
Contributors from top 500 universities

CLARIVATE ANALYTICS
BOOK CITATION INDEX
INDEXED

WEB OF SCIENCE™

Selection of our books indexed in the Book Citation Index in Web of Science™ Core Collection (BKCI)

Interested in publishing with us?
Contact book.department@intechopen.com

Numbers displayed above are based on latest data collected.
For more information visit www.intechopen.com

Chapter

Multiplexed Frequency-Selective Incoherent Holography

Wanbin Zhang, Baosheng Li and Jianquan Li

Abstract

We propose a new incoherent optical holographic spectrum stripping reconstruction method, called incoherent multiplexing frequency-selective holography, which compresses two or more on-axis holograms into a single multiplexed on-axis hologram without loss of magnification and resolution. The technique described in this chapter effectively suppresses the background bias term and conjugate term. The acquired spectrum is obtained by stripping in the overlapping confounding correlation terms. The experimental results show the potential of the method in areas such as compressed holography and extended field of view imaging.

Keywords: digital holography, multiplex holography, interferometric imaging, frequency modulation

1. Introduction

Multiplexed holography is the simultaneous capture of multiple complex wavefronts by a single CCD. Each wavefront is encoded into a hologram carrying different information. These complex wavefronts are compressed together and recorded at once. This is a tremendous improvement in acquisition efficiency, and multiplexed holography has the advantage of multiple field of view (FOV). Thus, multiplexed holography has many possible applications. Such as field-of-view multiplexing [1–7], depth-of-field multiplexing [8–12], non-scanning holographic lamination [13–16], and so on. In the development of holography, the laser has good coherence, and it is convenient to form holograms with the interferometer. Multiplexed holography first appeared in the field of coherent optical. In 2014, Frenklach et al. [17] proposed an interferometric method, called interferometry with a triple imaging area, where the camera acquires four holograms at once making the quantitative information collected in the camera exposure triple. In 2016, Rubin et al. [18] compressed six off-axis holograms into one multiplexed off-axis hologram without loss of magnification or resolution. And it can be reconstructed in the form of spatial filtering. The utilization of spatial bandwidth is greatly enhanced. In 2017, Dardikman et al. [19] used the space occupied by the DC term to place two pairs of complex wave fronts possessing conjugates. Eight holograms were reused in a single pass. The DC term needs to be removed by obtaining two phase-shifted holograms.

So far, the experimentally achievable coherent optical multiplexing can be extended to a maximum of eight holograms. The frequency domain obtained from the Fourier transform of the hologram shows that when the cutoff angular frequency required for the multiplexing method is four times the maximum angular frequency of the sample, the spectrum of the eight off-axis wave fronts already fills the two-dimensional frequency domain. No more wavefront spectrum can be accommodated. This is the reason for limiting the number of off-axis coherent optical multiplexes. Our incoherent optical multiplexing scheme can theoretically expand the number of multiplexed wavefronts to an infinite number of dimensions without considering reflectivity and transmittance losses. The frequency selection scheme in this paper needs to be implemented in combination with a single FINCH [20, 21] in a multi-beam setup.

2. Incoherent multiplexed frequency selection scheme

In Section 2, We describe in detail the scheme for stripping and reconstructing object-wave light from multiplexed complex wave fronts, arranged as follows: Section 2.1 presents the dual incoherent frequency selection scheme and experiments. Section 2.2 presents the triple incoherent frequency selection and experiments. Section 2.3 presents the arbitrary multiple incoherent frequency selection scheme. Section 2.4 discusses the advantages and potential developments of incoherent frequency selection over off-axis multiplexing.

2.1 Dual incoherent holographic frequency selection scheme and experiment

The experimental setup is shown in **Figure 1**, where the beam from a incoherent light source (CET-TCX250, 250 W) is passed through a narrow-band filter with a central wavelength of 20 nm. Collimated by a plano-convex lens. The focal length f_1 of the lens L is 150 mm. In the present frequency selection scheme, the polarization direction of the polarizer P is aligned with the long axis of the SLM, and the polarization direction is set to vertical. The symbols O and S in **Figure 1** represent the specimens measured on the two paths. The microscope objective (MO) on both branches serves to amplify the information of the object under test. The phase shifter in the optical path generates the experimentally required π phase shift of the corresponding object wave O(S). The two object beams are projected onto the spatial light modulator (SLM) (FSLM-2 K70-VIS, CAS Microstar) through the converging BS beam splitter on the right side. The mask loaded on the SLM is modulated according to the Fresnel wave band slice principle. The modulation equation can be expressed as $R(x, y) = \frac{1}{2} + \frac{1}{2}Q\left(-\frac{1}{a}\right)e^{i\theta}$. where $Q(b) = \exp\left[i\pi b\lambda^{-1}(x^2 + y^2)\right]$ denotes the quadratic phase function. Only about half of the incident light intensity is modulated by the Fresnel mask, while the remaining half is reflected without any modulation, which is the key to FINCH [20, 21]. The monochrome CCD camera (MER-502-79U3M/C) has 2448×2048 pixels, a pixel size of 3.45 μm, and captures at 79 fps.

In this paper, we use the half-wave plate (HWP) as the phase shift module. When the fast axis direction of the HWP is the same as the polarizer polarization direction, the Jones in the optical path is expressed as

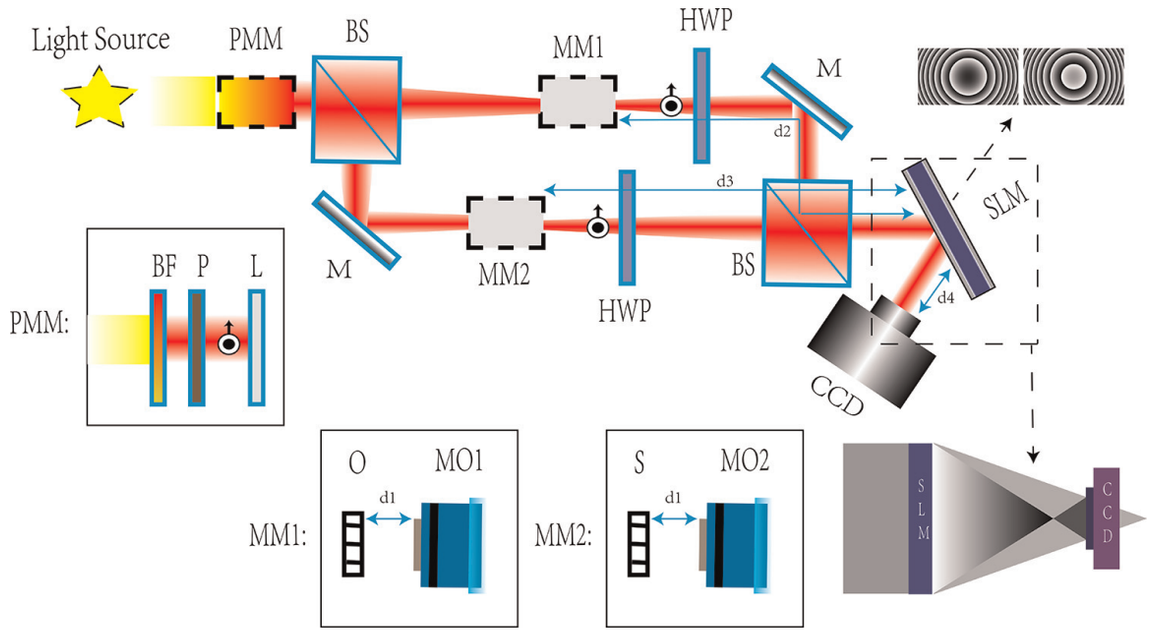

Figure 1.
TPFS-FINCH (two-pack frequency-selective-FINCH) optical multiplexing system. BF, bandpass filter; P, polarizer; PMM: Polarization modulation module; MM1: Microscopic objective module 1; MM2: Microscopic objective module 2; BS, beam splitter; MO, microscope objectives; HWP, half-wave plate; M, mirror; O, object; S, specimen; MO1, ×4, 0.1-NA; MO2, ×10, 0.25-NA; SLM, spatial light modulator; CCD, charge coupled device.

$$E_R = H \cdot E_v = \begin{bmatrix} 1 & 0 \\ 0 & -1 \end{bmatrix} \begin{bmatrix} 0 \\ 1 \end{bmatrix} = \begin{bmatrix} 0 \\ -1 \end{bmatrix} = \begin{bmatrix} 0 \\ e^{i\pi} \end{bmatrix}, \tag{1}$$

where H is the Jones representation of the HWP, and E_v is the Jones representation of the linearly polarized light after passing through the polarizer. According to the Fresnel diffraction theory, the light intensity of the two transmitted samples of light reaching the sensor surface can be expressed as.

$$I_1 = \left| \frac{1}{2} Q\left(\frac{1}{\alpha + d_4}\right) + \frac{1}{2} Q\left(\frac{1}{d_4 - {}^{\alpha a}/_{\alpha - a}}\right) e^{i\theta} \right|^2 \tag{2}$$

$$I_2 = \left| \frac{1}{2} Q\left(\frac{1}{\beta + d_4}\right) + \frac{1}{2} Q\left(\frac{1}{d_4 - {}^{\beta a}/_{\beta - a}}\right) e^{i\theta} \right|^2. \tag{3}$$

Where $\alpha^{-1} = \left(f_{mo1} - d_1\right) / \left[f_{mo1}(d_1 + d_2) - d_1 d_2\right]$ and $\beta^{-1} = \left(f_{mo2} - d_1\right) / \left[f_{mo2}(d_1 + d_3) - d_1 d_3\right]$. The distance parameters in the two-pack frequency-selective (TPFS) experiment are a = 150 mm, d1 = 7 mm, d2 = d3 = 235 mm and d4 = 56 mm.

In the frequency selection scheme, if the two holograms are just intensity superimposed, the combined hologram received by the camera should be $I = I_1 + I_2$. If the dual path setup if the conditions of the Mach–Zehnder interferometer are satisfied, the multiple holography recorded by the CCD is an incoherent superposition of all object point intensities by analyzing the interference intensity distribution of the infinite elements, for two three-dimensional objects $g_0(x_0, y_0, z_0)$ and $g_s(x_s, y_s, z_s)$:

$$E(x,y) \cong A\left[C + \iiint g_0(x_0,y_0,z_0)Q\left(\frac{1}{d_4 - \frac{\alpha a}{\alpha - a}} + \frac{1}{\alpha + d_4}\right)e^{i\theta}dx_0dy_0dz_0\right. \tag{4}$$

$$+ \iiint g_0(x_0,y_0,z_0)Q\left(\frac{1}{\alpha + d_4} + \frac{1}{d_4 - \frac{\alpha a}{\alpha - a}}\right)e^{-i\theta}dx_0dy_0dz_0$$

$$+ \iiint g_s(x_s,y_s,z_s)Q\left(\frac{1}{d_4 - \frac{\beta a}{\beta - a}} - \frac{1}{\beta + d_4}\right)e^{i\theta}dx_sdy_sdz_s$$

$$+ \iiint g_s(x_s,y_s,z_s)Q\left(\frac{1}{\beta + d_4} - \frac{1}{d_4 - \frac{\beta a}{\beta - a}}\right)e^{-i\theta}dx_sdy_sdz_s$$

$$+ \iiint g_0(x_0,y_0,z_0)Q\left(\frac{1}{d_4 - \frac{\alpha a}{\alpha - a}}\right)e^{i\theta}dx_0dy_0dz_0$$

$$+ \iiint g_s(x_s,y_s,z_s)Q\left(\frac{-1}{d_4 - \frac{\beta a}{\beta - a}}\right)e^{-i\theta}dx_sdy_sdz_s$$

$$+ \iiint g_0(x_0,y_0,z_0)Q\left(\frac{-1}{d_4 - \frac{\alpha a}{\alpha - a}}\right)e^{-i\theta}dx_0dy_0dz_0$$

$$\left. + \iiint g_s(x_s,y_s,z_s)Q\left(\frac{1}{d_4 - \frac{\beta a}{\beta - a}}\right)e^{i\theta}dx_sdy_sdz_s\right].$$

In order to implement two-pack frequency-selective FINCH (TPFS-FINCH), the corresponding experimental steps are as follows:

1. When a(b) of **Figure 2** is loaded on the SLM and the both phase shift modules do not apply phase shift to the target beam, the intensity distribution recorded by the CCD is E_{10} (E_{20}).

2. Applying a phase shift π exclusively to the object-wave O, i.e. multiplying the object-wave O by the phase factor $e^{i\pi}$. The CCD collected E_{11} and E_{21} intensity distributions after loading a and b of **Figure 2** on the SLM, respectively.

3. On the object wave S, just the phase shift π is applied. The intensity distributions recorded by the CCD are E_{12} and E_{22}, and the phase mask loaded on the SLM is compatible with step (1).

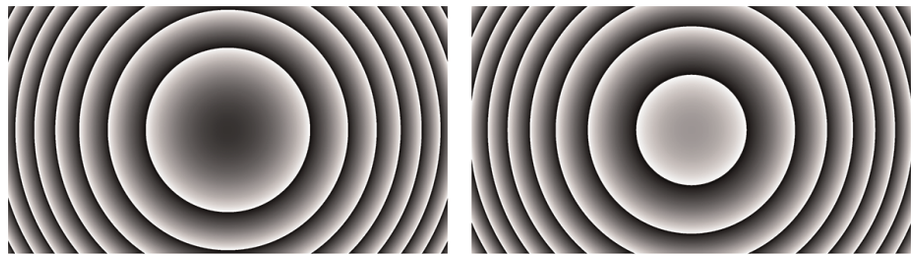

Figure 2.
(a) Fresnel mask template with a gray value of 31. (b) Fresnel mask template with a gray value of 154.

4. The phase shift π is applied to both the object waves O and S at the same time. The phase mask loaded on the SLM is consistent with step (1), and the CCD captured E_{13} and E_{23} intensity distributions.

In TPFS, we take into account the presence of intensity superposition and incoherent optical interference and can remove the spectral information of the object O by the following equation:

$$FT\{O\} = \frac{FT\left\{\frac{1}{4}(E_{20} - E_{21} + E_{22} - E_{23})\right\}H_{-z_1} - FT\left\{\frac{1}{4}(E_{10} - E_{11} + E_{12} - E_{13})\right\}H_{-z_2}}{2(H_{z_2-z_1} - H_{z_1-z_2})}, \tag{5}$$

$$FT\{S\} = \frac{FT\left\{\frac{1}{4}(E_{20} + E_{21} - E_{22} - E_{23})\right\}H_{-z_1} - FT\left\{\frac{1}{4}(E_{10} + E_{11} - E_{12} - E_{13})\right\}H_{-z_2}}{2(H_{z_2-z_1} - H_{z_1-z_2})}. \tag{6}$$

At last, when reconstructing the object information of the corresponding respective branches, the transfer function $H_z\left(f_x, f_y, z_i\right) = \exp\left[ikz_i\sqrt{1-\left(\lambda f_x\right)^2 - \left(\lambda f_y\right)^2}\right]$ intercorrelation reconstruction in angular spectral diffraction theory is used. As shown in **Figure 3**.

As can be seen from **Figure 3**, **Figure 3**(e) and (f) are the complex wave fronts reconstructed by stripping from the multiplexed hologram **Figure 3**(d). The intensity distribution of the red solid line also clearly demonstrates that the numbers 4 and 6 have been separated from the compressed hologram. Two-branch multiplexed hologram separation reconstruction has been performed without decreasing the resolution and without increasing the noise.

2.2 Triple incoherent holographic frequency selection scheme and experiment

After successfully implementing the scheme of TPFS-FINCH in the incoherent domain, is it possible to implement the extension of dual frequency selection by adding a dimension to triple frequency selection? This is what needs to be explored in this subsection.

As shown in **Figure 4**, a figure of the experimental setup with triple frequency selection is shown here. The difference from the setup in **Figure 1** is that there is one

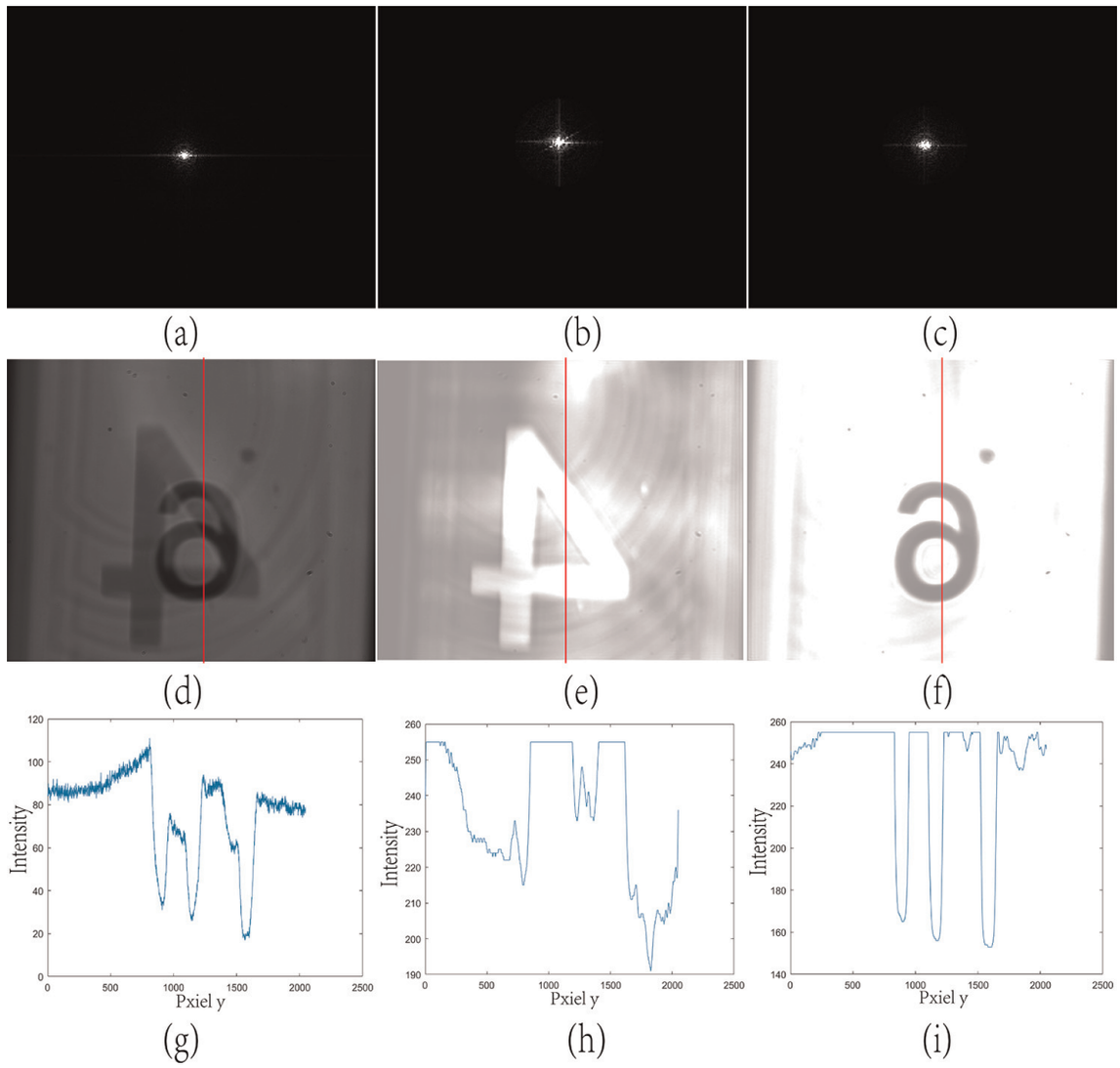

Figure 3.
(a) To (c) the power spectra of (d), (e) and (f), respectively. (e) and (f) the wavefront reconstructed from (d) by means of spectral separation. (g) To (i) the intensity distributions of the red solid lines in the (d)-(f), respectively.

more path carrying information about the object wave light. The phase shifter and phase mask template are the consistent. The experimental steps are as follows.

1. **Figure 2**(a) is loaded onto the SLM with no HWP loaded on all three branches and the intensity distribution captured on the CCD is E_{10}. Placing the phase shifter on the first branch generates a phase shift and the intensity distribution received on the CCD is E_{11}. Placing the phase shifter on the second branch to produce a phase shift, the intensity distribution picked up on the CCD is E_{12}. Placing the phase shifter on the third branch to produce a phase shift, the intensity distribution received on the CCD is E_{13}.

2. **Figure 2**(b) is loaded onto the SLM without HWP on all three branches, and the intensity distribution acquired on the CCD is E_{20}. Placing the phase shifter on the first branch generates a phase shift, and the intensity distribution received on the CCD is E_{21}. Placing the phase shifter on the second branch produces a phase shift, and the intensity distribution picked up on the CCD is E_{22}. Placing the phase

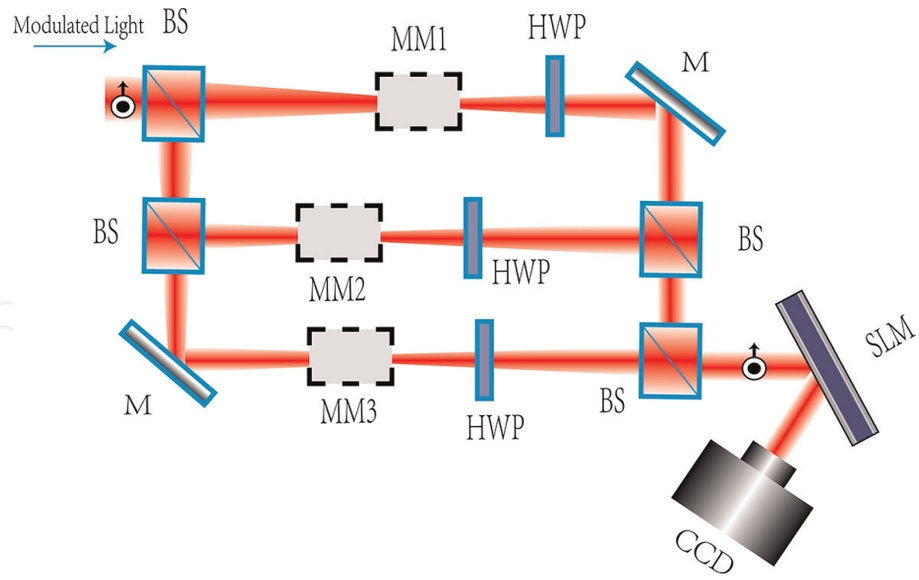

Figure 4.
Triple incoherent holographic frequency selection setup.

shifter on the third branch produces a phase shift, and the intensity distribution pictured on the CCD is E_{23}.

Combined with the multiplexed holograms acquired by the camera, the wavefront spectra of objects S_1, S_2 and S_3 can be stripped out by Eq. (7). Then reconstructed with the spatial transfer function $H_z\left(f_x, f_y, z_i\right)$ correlation.

$$FT\{S_n\} = \frac{FT\{E_{20} - E_{2n}\}H_{-z_1} - FT\{E_{10} - E_{1n}\}H_{-z_2}}{2(H_{z_2-z_1} - H_{z_1-z_2})}, n = 1,2,3. \tag{7}$$

The experimental results of three-pack frequency-selective FINCH are shown in **Figure 5**. The numbers 5, 2, and 6 have been separated from the compressed hologram **Figure 5**(e) and the angular spectrum reproduced.

2.3 Arbitrary multiplexed incoherent holographic frequency selection theory scheme

In the field of coherent optical multiplexing, when the idea of multiplexing two channels is further developed to six channels [18], the spectral position in the spatial frequency domain needs to be calculated precisely. And the cross term between the mismatched sample beam and the reference beam should be avoided. These cross terms occupy space in the spatial spectrum required for the additional wavelength channels. Because of the limited spatial frequency domain, the development of coherent optical holographic multiplexing came to an abrupt end at 8PH. The frequency spectrum of the zero-order term and the conjugate term of the incoherent optical in-axis self-interference holography overlap together and can co-occupy the position with the center of the frequency domain. This theoretically eliminates the need to consider how to filter by means of spatial filtering. Using the frequency selection scheme described in this paper the spectrum that is desired to be reconstructed can be stripped out by means of an equation calculation. Based on the experiments of

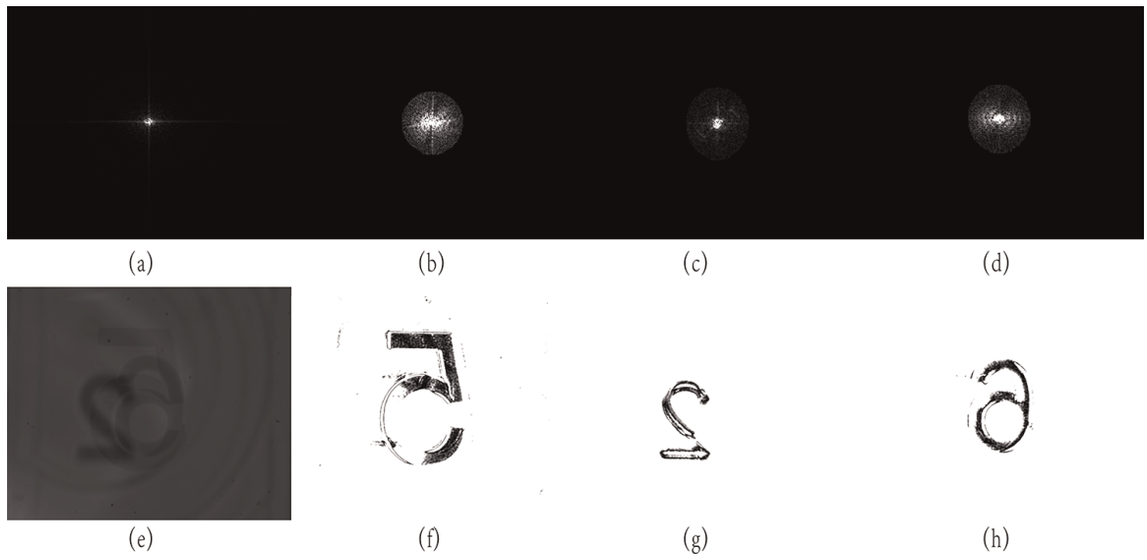

Figure 5.
(a) To (d) the power spectra of (e), (f), (g) and (h), respectively. (f)-(h) is the angular spectrum reproduced by separating the reconstruction from the compressed hologram (e).

multiplexing in Sections 2.1 and 2.2, this subsection describes the theoretical scheme based on the implementation of frequency selection under arbitrary multi-beam settings.

In an arbitrary multiplexed holographic intensity superposition setup, the multiplexed hologram of the n-th branch producing a phase shift when the SLM is loaded with mask a is denoted by E_{an}. Similarly, E_{bn} is used to indicate the multiplexed hologram of the n-th branch generating the phase shift when the SLM is loaded with mask b. E_{a0} and E_{b0} denote multiplexed holograms with all branches not loaded with phase shifts. S_n corresponds to the spectrum of the object wave on the n-th branch.

The equation for the spectrum of the object wave on an arbitrary branch can be expressed as:

$$FT\{S_n\} = \frac{FT\{E_{b0} - E_{bn}\}H_{-z_1} - FT\{E_{a0} - E_{an}\}H_{-z_2}}{2(H_{z_2-z_1} - H_{z_1-z_2})}. \tag{8}$$

At this stage, the arbitrary multiplexed incoherent multiplexing holographic frequency selection scheme has been completed.

2.4 Comparison and discussion

The frequency selection scheme in this paper is compared with studies in the field of coherent light [16–18, 22–27], where a multiplexed holography scheme for coherent light projects two interferometric patterns with different stripe orientations onto the camera, each capturing a different region of the sample or a complex wave front of a different sample. This technique is called interferometry with double imaging area. Since the two FOVs in the coherent light field do not overlap in the spatial frequency domain, they can be completely reconstructed and stitched together without loss of resolution or magnification. The effect of frequency selection is experimentally demonstrated in Sections 2.1 and 2.2 of this paper. The corresponding wavefront spectrum is calculated by Equation. The reconstruction also does not lose resolution and

amplification as long as the phase shift is accurate. Stitching different wavefronts together after reconstruction can achieve a multiplexed field of view after reconstructing static or dynamic samples.

According to the calculation of wavefront acquisition efficiency [19], the efficiency of any n-way multiplexed holographic frequency selection is n/8. For in-axis FINCH, a single acquisition of the object wavefront generally requires a three-step phase shift technique to eliminate the conjugate and DC terms. Acquiring n wavefronts requires 3n holograms. Therefore, for the incoherent frequency selection scheme in this paper, the wavefront acquisition improves the efficiency by a factor of 3n/8. Obviously, when n > =3, the advantage of the frequency selection technique of increasing the acquisition efficiency on the basis of ensuring the original FOV of the camera becomes apparent. Frequency selective operation allows us to obtain multiplexed imaging FOVs without adjusting the time interval captured in each sub-hologram to the camera's frame rate. This is particularly effective for situations where the spatial resolution of a static observer is insufficient.

3. Summary

This chapter describes the frequency selection principles and experimental requirements for incoherent multiplexing. The combination of wavefront interference and single-channel FINCH techniques allows a completely new approach to frequency selection. The frequency selection method and the off-axis multiplexing method are compared and analyzed in terms of FOV, efficiency, and applicable scenarios. In general, the incoherent frequency selection principle is expected to be used for a wide range of applications that focus on the advantages of compressed holographic data and incoherent light, including multiplexed field-of-view imaging, fluorescence imaging, and structured light super-resolution imaging.

Acknowledgements

We thank Professor Joseph Rosen for his review comments on this chapter. We sincerely thank Chunlin Shi and Jinjin Song for their assistance with this experiment. Appreciation is extended to Ms. Rongyu Wang and Yimu Zhang for their support to the authors in writing this chapter.

Funding

This work is supported by the Natural Science Foundation of China (NSFC) under Grant Nos. 52177137 and 41371336.

IntechOpen

Author details

Wanbin Zhang[1,2*], Baosheng Li[1,2] and Jianquan Li[1,2]

1 School of Instrument Sciences and Opto-Electronics Engineering, Hefei University of Technology, Hefei, China

2 Anhui Province Key Laboratory of Measuring Theory and Precision Instrument, Hefei University of Technology, Hefei, Anhui, China

*Address all correspondence to: wbzhang0419@163.com

IntechOpen

© 2022 The Author(s). Licensee IntechOpen. This chapter is distributed under the terms of the Creative Commons Attribution License (http://creativecommons.org/licenses/by/3.0), which permits unrestricted use, distribution, and reproduction in any medium, provided the original work is properly cited. CC BY

References

[1] Mirsky SK, Shaked NT. First experimental realization of six-pack holography and its application to dynamic synthetic aperture superresolution. Optics Express. 2019;**27**: 26708-26720

[2] Girshovitz P, Frenklach I, Shaked NT. Broadband quantitative phase microscopy with extended field of view using off-axis interferometric multiplexing. Journal of Biomedical Optics. 2015;**20**:111217

[3] Rotman-Nativ N, Turko NA, Shaked NT. Flipping interferometry with doubled imaging area. Optics Letters. 2018;**43**:5543-5546

[4] Girshovitz P, Shaked NT. Doubling the field of view in off-axis low-coherence interferometric imaging. Light Science Applications. 2014;**3**:e151

[5] Roitshtain D, Turko NA, Javidi B, Shaked NT. Flipping interferometry and its application for quantitative phase microscopy in a micro-channel. Optics Letters. 2016;**41**:2354-2357

[6] Tahara T, Awatsuji Y, Nishio K, Ura S, Matoba O, Kubota T. Space-bandwidth capacity-enhanced digital holography. Applied Physics Express. 2013;**6**:22502

[7] Zhang W, Li B, Shi C, Li J. Two-pack frequency-selective incoherent holography by using a dual-beam setup. Optics and Lasers in Engineering. 2022; **156**:107086

[8] Dalgarno PA, Dalgarno HIC, Putoud A, Lambert R, Paterson L, Logan DC, et al. Multiplane imaging and three dimensional nanoscale particle tracking in biological microscopy. Optics Express. 2010;**18**:877-884

[9] Rai MR, Rosen J. Depth-of-field engineering in coded aperture imaging. Optics Express. 2021;**29**:1634-1648

[10] Maurer C, Khan S, Fassl S, Bernet S, Ritsch-Marte M. Depth of field multiplexing in microscopy. Optics Express. 2010;**18**:3023-3034

[11] Ferraro P, Paturzo M, Memmolo P, Finizio A. Controlling depth of focus in 3D image reconstructions by flexible and adaptive deformation of digital holograms. Optics Letters. 2009;**34**: 2787-2789

[12] Kostencka J, Kozacki T, Li˙zewski K. Autofocusing method for tilted image plane detection in digital holographic microscopy. Optics Communication. 2013;**297**:20-26

[13] Schilling BW, Poon T-C, Indebetouw G, Storrie B, Shinoda K, Suzuki Y, et al. Three-dimensional holographic fluorescence microscopy. Optics Letters. 1997;**22**(19):1506-1508

[14] Fang-Yen CM, Choi W, Sung Y, Holbrow CJ, Dasari RR, Feld MS. Video-rate tomographic phase microscopy. Journal of Biomedical Optics. 2011;**16**: 011005

[15] Jin D, Zhou R, Yaqoob Z, So PTC. Dynamic spatial filtering using a digital micromirror device for high-speed optical diffraction tomography. Optics Express. 2018;**26**:428-437

[16] Kim K, Yoon J, Park Y. Simultaneous 3D visualization and position tracking of optically trapped particles using optical diffraction tomography. Optica. 2015;**2**: 343-346

[17] Frenklach I, Girshovitz P, Shaked NT. Off-axis interferometric

phase microscopy with tripled imaging area. Optics Letters. 2014;**39**:1525-1528

[18] Rubin M, Dardikman G, Mirsky SK, Turko NA, Shaked NT. Six-pack off-axis holography. Optics Letters. 2017;**42**: 4611-4614

[19] Dardikman G, Shaked NT. Is multiplexed off-axis holography for quantitative phase imaging more spatial bandwidth-efficient than on-axis holography? Journal of the Optical Society of America. A. 2019;**36**:A1-A11

[20] Rosen J, Brooker G. Digital spatially incoherent fresnel holography. Optics Letters. 2007;**32**:912-914

[21] Rosen J, Brooker G. Fluorescence incoherent color holography. Optics Express. 2007;**15**:2244-2250

[22] Fugal PJ, Shaw RA, Saw EW, Sergeyev AV. Airborne digital holographic system for cloud particle measurements. Applied Optics. 2004;**43**: 5987-5995

[23] Schnell M, Perez-Roldan MJ, Carney PS, Hillenbrand R. Quantitative confocal phase imaging by synthetic optical holography. Optics Express. 2014;**22**:15267-15276

[24] Balasubramani V, Tu H, Lai X, et al. Adaptive wavefront correction structured illumination holographic tomography. Scientific Reports. 2019;**9**: 10489

[25] Rosen J, Vijayakumar A, Kumar M, Rai MR, Kelner R, Kashter Y, et al. Recent advances in self-interference incoherent digital holography. Advances in Optics and Photonics. 2019;**11**:1-66

[26] Wan Y, Liu C, Ma T, Qin Y, Lv S. Incoherent coded aperture correlation holographic imaging with fast adaptive and noise-suppressed reconstruction. Optics Express. 2021;**29**:8064-8075

[27] Vijayakumar A, Rosen J. Spectrum and space resolved 4D imaging by coded aperture correlation holography (COACH) with diffractive objective lens. Optics Letters. 2017;**42**:947-950